International Journal of Nanomedicine

Dovepress
Taylor & Francis Group

Open Access Full Text Article

ORIGINAL RESEARCH

USC-Derived Small Extracellular Vesicles-Functionalized Scaffolds Promote Scarless Vaginal Defect Repair via Delivery of Decorin and DUSP3 Proteins

Yiyun Xu[1,*], Jie Li[1,*], Yu Qiu[1], Fuyue Wu[2], Zhuowei Xue[1], Bin Liu[1], Hongjie Fan[1], Yuedi Zhou[1], Qingkai Wu[1]

[1]Department of Obstetrics and Gynecology, Shanghai Sixth People's Hospital Affiliated to Shanghai Jiao Tong University School of Medicine, Shanghai, 200233, People's Republic of China; [2]Organoid Regeneration Research Center, ReMed Regenerative Medicine Clinical Application Institute, Shanghai, 201114, People's Republic of China

*These authors contributed equally to this work

Correspondence: Qingkai Wu; Yuedi Zhou, Email wuqingkai@sjtu.edu.cn; zhouyuedi@126.com

Background: Scar formation following large-area vaginal defects post-vaginoplasty is a major clinical challenge. Compared to skin scars, vaginal scars can lead to pain during intercourse and urinary difficulties, severely impacting quality of life. Small extracellular vesicles (sEVs) encapsulate diverse bioactive components, making them potential therapeutic agents. Designing functional scaffolds that incorporate sEVs is a promising approach for scarless vaginal defect repair.

Methods: sEVs-loaded scaffolds were developed through electrostatic interactions between negatively charged sEVs secreted by urine-derived stem cells (USC-sEVs) and positively charged human acellular amniotic membranes. The efficacy of sEVs-loaded scaffolds in the treatment of vaginal defects in rabbits was assessed by histological analysis. Immunofluorescence staining, Western blot, qRT-PCR and collagen gel contraction analyses were conducted to evaluate the antifibrotic effects of USC-sEVs. RNA sequencing was employed to elucidate the underlying mechanisms involved. LC–MS/MS analysis was used to identify candidate upstream proteins in USC-sEVs.

Results: In vivo experiments demonstrated that the sEVs-loaded scaffolds promoted scarless healing of vaginal defects in rabbits by modulating collagen deposition, reducing fibrosis, and diminishing inflammation. In vitro experiments revealed that USC-sEVs significantly inhibited the proliferation, collagen production, and activation of fibroblasts with a fibrotic phenotype, indicating the antifibrotic properties of USC-sEVs. Transcriptome and Western blot analyses revealed that USC-sEVs treatment inhibited fibrosis by downregulating the TGF-β and p38 MAPK signaling pathways. LC–MS/MS analysis identified 2653 proteins encapsulated in USC-sEVs. Western blot analysis revealed that decorin, an inhibitor of the TGF-β signaling pathway, and DUSP3, a negative regulator of p38 phosphorylation, were enriched in USC-sEVs and could be transferred to fibroblasts.

Conclusion: USC-sEVs inhibited fibrosis and promoted scarless healing by delivering decorin and DUSP3 proteins, which regulate the TGF-β and p38 MAPK signaling pathways, respectively. This study highlights the potential of sEVs-loaded scaffolds as a promising strategy for scarless vaginal repair following vaginoplasty, offering a novel approach for regenerative medicine with significant translational potential for clinical application.

Keywords: small extracellular vesicles, urine-derived stem cells, vaginal defects, scarless repair, anti-fibrosis

Introduction

Vaginoplasty is a surgical procedure used to reconstruct the vagina and is primarily indicated for patients with congenital vaginal atresia, those who have undergone extensive resection due to malignant vaginal tumors, and individuals who have undergone sex reassignment surgery.[1] The most common surgical approach involves creating an artificial space

Received: 18 October 2024
Accepted: 23 January 2025
Published: 5 February 2025

Graphical Abstract

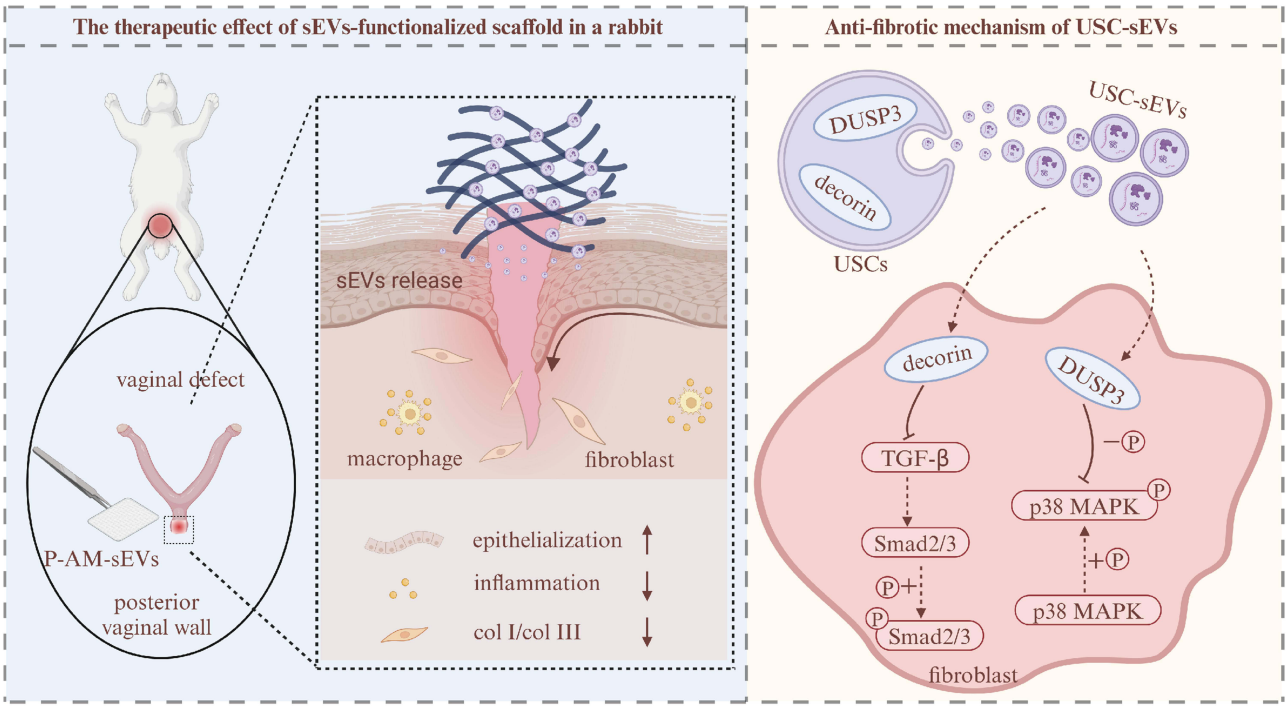

between the rectum and bladder, where an inner lining material is placed.[2] Based on the type of inner lining material used, vaginoplasty can be categorized into peritoneal flap vaginoplasty, intestinal vaginoplasty, and buccal mucosa vaginoplasty, among others.[3,4] However, the use of autologous tissue is limited due to its scarcity and the increased morbidity at the donor site.[5] In recent years, tissue-engineered materials have been studied as alternatives to autologous tissue for vaginal repair. Natural tissue-derived patches, such as animal-derived acellular dermal matrix and decellularized small intestinal submucosa (SIS), might encounter issues of graft contraction and prolong epithelialization time.[6,7] Synthetic polymer-based patches, such as bilayer silk fibroin, were found to be prone to chronic inflammatory reactions and fibrosis upon long-term implantation, which could ultimately lead to vaginal stenosis.[8] Additionally, cell-seeded scaffolds, such as skeletal muscle-derived stem cells seeded on SIS scaffolds, faced challenges related to cell sourcing, cell expansion, and scaffold component selection.[9] Currently, there is a lack of an ideal artificial vaginal lining material in clinical practice that can effectively address these issues and achieve satisfactory repair outcomes.

The wounds following vaginoplasty are characterized by significant depth and large surface area, with epithelialization taking several months. Common postoperative issues include vaginal stenosis, insufficient length, poor elasticity, and discomfort during intercourse, all of which are primarily attributed to scar tissue formation during the healing process.[10,11] Scar formation not only affects the appearance and physiological function of the newly reconstructed vagina but may also increase the psychological burden on patients.[12] Achieving scar-free healing is crucial for improving clinical outcomes in vaginoplasty, yet research on promoting scarless healing in vaginal reconstruction remains limited. Therefore, the development of tissue-engineered scaffolds that can accelerate scarless vaginal healing and allow for personalized treatment is a research direction with potential clinical application value.

Small extracellular vesicles (sEVs) are rich in bioactive molecules such as proteins, lipids, RNAs, and other small molecules, which can be transferred to target cells and participate in intercellular communication.[13] Compared with direct stem cell transplantation, stem cell-derived sEVs may avoid potential risks such as immune rejection, tumorigenicity, and instability, making them increasingly attractive options as potential therapeutic agents.[14] Autologous urine-derived stem cells (USCs) offer several advantages, including ease of collection, abundant availability, non-invasive and painless

procedures, and low immunogenicity.[15] Moreover, during embryonic development, USCs exhibit a high degree of homology with the urogenital system.[16] Therefore, USC-derived sEVs (USC-sEVs) present unique advantages in vaginal tissue regeneration. In this study, we designed to load sEVs onto scaffolds to prolong their retention at the wound site.

Inspired by the scarless healing properties of fetal wound, this study chose the natural fetal membrane, the amniotic membrane (AM), as a scaffold.[17] The AM contains extracellular matrix (ECM) components such as collagen, laminin, and fibronectin, which provide a three-dimensional scaffold structure favorable for cell adhesion, proliferation, and migration.[18] The unique physiological environment of the vagina, including an acidic pH (3.8–4.5), a healthy microbiome, and sufficient moisture, plays a critical role in vaginal repair.[19] The AM contains anti-inflammatory factors and antimicrobial agents, thereby contributing to maintaining the vaginal acidic environment and supporting the restoration of a healthy vaginal microbiome.[20] Additionally, USC-sEVs also have anti-inflammatory properties.[21] The wettability and favorable permeability of the AM help maintain appropriate moisture in the vaginal repair area, further supporting the healing process.

This study developed an AM scaffold loaded with USC-sEVs, which promoted scarless healing of the vaginal wall in rabbits. Further in vitro experiments firstly indicated that USC-sEVs might inhibit fibrosis by delivering decorin and DUSP3 proteins to fibroblasts. Successful development of vaginal repair scaffolds has broad potential implications in the field of tissue engineering, particularly by providing new therapeutic strategies for the repair of organs such as the urethra, bladder, and skin. The selection of scaffolds and the active components they carry, especially for tissues affected by conditions like fibrosis and scarring, offer new perspectives for tissue repair. This research studied the feasibility of the sEVs-loaded scaffold in a rabbit model, but further studies in more clinically relevant models or human trials are required. Such advancements are crucial for advancing tissue engineering therapies towards clinical application.

Methods

Isolation, Culture and Identification of USCs

Human urine samples were collected from healthy women who underwent full-term cesarean sections at the Department of Obstetrics and Gynecology, Shanghai Sixth People's Hospital. Written informed consent was obtained from all donors prior to sample collection and use. All procedures were approved by the Independent Ethics Committee of Shanghai Sixth People's Hospital (Approval code: 2018-KY-035(K)). All procedures were conducted in accordance with the Declaration of Helsinki. USCs were isolated from the urine samples of healthy women as previously described.[22,23] USCs at passages 3–6 were used for subsequent experiments. Flow cytometric analysis was performed to assess the surface markers of the USCs. Following trypsin digestion, USCs were resuspended in phosphate-buffered saline (PBS, Servicebio, China) containing 1% fetal bovine serum (FBS, Gibco, USA), and incubated with antibodies (BD Biosciences, USA) at 4°C for 30 minutes. The surface antigens of USCs were then detected via a flow cytometer (Beckman Coulter, USA). The antibodies used were as follows: CD29 (1:100, 561,795), CD44 (1:100, 560,977), CD45 (1:100, 564,106), CD73 (1:100, 560,847), and HLA-DR (1:100, 560,943).

Isolation and Identification of USC-sEVs

USC-sEVs were isolated from USC culture supernatants via differential centrifugation and ultracentrifugation following a previously published protocol.[23] For removal of necrotic cellular debris, the medium was sequentially centrifuged at 300 × g for 15 minutes, 2000 × g for 30 minutes, and 10000 × g for 60 minutes, followed by filtration through 0.22 μm sterile filters (Millipore, USA). Then, to collect sEVs, the medium was ultracentrifuged twice at 100,000 × g for 70 minutes, using a Beckman Coulter Optima XPN-100 ultracentrifuge equipped with a Type 70 Ti fixed-angle rotor (Beckman Coulter). The pellet was resuspended in PBS. Transmission electron microscopy (TEM, Thermo Scientific, USA) was used to observe the morphology of USC-sEVs. A small volume of vesicle suspension was placed onto a copper grid, followed by negative staining with phosphotungstic acid solution (2% w/v). The sample was air-dried at room temperature before being examined and photographed under a TEM. Nanoparticle tracking analysis (NTA, Particle Metrix, Germany) was employed to determine the size distribution and particle concentration of USC-sEVs. The zeta potential of USC-sEVs was measured via a ZetaView instrument.

Fabrication and Characterization of sEVs-Functionalized Scaffolds

Fresh amniotic membranes (AMs) were obtained from healthy women who underwent full-term cesarean sections at the Department of Obstetrics and Gynecology, Shanghai Sixth People's Hospital. Written informed consent was obtained from all donors prior to sample collection and use. All procedures were approved by the Independent Ethics Committee of Shanghai Sixth People's Hospital (Approval code: 2018-KY-035(K)). All procedures were conducted in accordance with the Declaration of Helsinki. A unidirectional decellularization method was employed to preserve the stromal layer of the AM effectively while removing the epithelial cells, yielding a high-quality decellularized AM product. Fresh AMs were laid flat, with the epithelial surface exposed to Trypsin-like enzyme and nuclease treatment solutions. The membranes were then sterilized via ethanol and gamma irradiation, and stored in glycerol at 4°C.

Owing to the negative charge on the surface of sEVs, this study treated wet-state acellular amniotic membrane with a polyethyleneimine (PEI) solution to impart a positive charge, enabling the fabrication of a functionalized bio-scaffold through electrostatic interactions. For covalent conjugation of PEI, the trimmed 1.5 cm × 1.5 cm AM segments were immersed in 2-(N-morpholino) ethanesulfonic acid buffer (pH 5.5) containing 0.1 M 1-ethyl-3-(3-dimethylaminopropyl) carbodiimide (EDC) and 0.05 M N-hydroxysuccinimide (NHS) at room temperature for 1 hour. The activated AM was removed from the EDC/NHS solution and immersed in a 2 mg/mL branched PEI (Beyotime, China) solution at room temperature for 12 hours. The positively charged AM was removed from the PEI solution and washed with PBS to remove unbound PEI. The membrane was then immersed in 1 mL of a negatively charged USC-sEVs solution at a concentration of 10×10^{10} particles/mL and incubated with gentle agitation at 4°C for 12 hours. The membrane was subsequently used for further experiments.

The in vitro release of particles from the sEVs-loaded scaffolds was analyzed via NTA. The sEVs-loaded scaffold was immersed in PBS, and the number of sEVs particles continuously released from the scaffold was measured at various time points. The uptake of DiR-labeled USC-sEVs in vivo was described in Supplementary Information 1. The microstructures of the AMs and cell-seeded AMs were observed via scanning electron microscopy (SEM, Hitachi, Japan). The samples were dehydrated, dried, sputter-coated with gold, and then imaged via SEM. The biocompatibility of the AMs was assessed via a live/dead cell staining assay kit (Beyotime). An AM was placed at the bottom of the culture plates, and the fibroblasts were seeded onto the AM membrane. After 36 hours of incubation, calcein acetoxymethyl ester (AM)/propidium iodide (PI) working solution was added, and the cells were incubated at 37°C in the dark for 30 minutes. Calcein AM was used to stain live cells, which emitted green fluorescence, whereas PI was used to stain dead cells, which emitted red fluorescence. The hemolysis test to assess the hemolytic rates of different samples was described in Supplementary Information 1.

Establishment and Treatment of a Vaginal Defect Model in Rabbits

The animal experiments in this study were approved by the Animal Care and Use Committee of Shanghai Sixth People's Hospital (No. 2023–0517). All animal experiments were conducted in accordance with the ethical review of animal welfare for laboratory animals (GB/T 35892–2018). Multiparous New Zealand white female rabbits weighing 4.0–4.5 kg were used in the study. The species was selected because its capacious vaginal conditions are particularly suitable for vaginal surgery. The rabbits were anesthetized, and the hair around the vulva was shaved. All surgical procedures were performed under sterile conditions. A vaginal defect approximately 1 cm × 1 cm in size was created in the posterior vaginal wall under direct visualization. The excised tissue included the vaginal epithelium, smooth muscle and connective tissue. The in vivo experimental design was as follows. In the control group, the vaginal defects were treated with sterile PBS. In the AM group, the vaginal defects were covered with AMs. In the sEVs group, USC-sEVs, equivalent to the amount loaded onto AMs with sEVs, were applied to the surface of the vaginal defects. In the sEVs-loaded scaffold group, AMs loaded with USC-sEVs were applied to the defect sites.

Histological and Immunostaining Analysis

The rabbits were euthanized at the appointed time, and the full-thickness posterior vaginal wall was collected from the different groups. The tissues were fixed in 4% paraformaldehyde (PFA), dehydrated and embedded in paraffin. The

vaginal tissues were sectioned at a thickness of 5 μm for staining. The sections were subjected to hematoxylin and eosin (H&E) staining or Picrosirius red staining. For immunohistochemistry (IHC) staining, the sections were incubated with anti-collagen III (1:200; Novus, USA, NBP1-05119) and anti-Interleukin-6 (IL-6) (1:300; Proteintech, China, 21865-1-ap) antibodies overnight at 4°C. The following day, the sections were treated with a biotinylated secondary antibody and avidin-biotin-peroxidase, followed by visualization with diaminobenzidine. Finally, the sections were counterstained with hematoxylin. For immunofluorescence (IF) staining, the sections were incubated with anti-CD68 (1:50; Abcam, UK, ab955) antibody overnight at 4°C in the dark. Then, the sections were incubated with the secondary antibody at room temperature for 1 h. Images were acquired via a microscope.

Culture and Experimental Protocol of Fibroblasts

Human skin fibroblasts (BJ cells) were purchased from iCell Bioscience Co., Ltd. (Shanghai, China), and cultured in minimum essential medium supplemented with 10% FBS and 1% penicillin–streptomycin. BJ cells were treated with 10 ng/mL transforming growth factor beta 1 (TGF-β1, PeproTech, USA, Cat# 100–21C) for 24 h to induce a fibrotic phenotype, and the culture medium was replaced. After fibrotic phenotype induction, the BJ cells were further incubated with fresh medium containing USC-sEVs (5×10^9 particles/mL) or PBS for an additional 48 h.

Proliferation Assay

Cell proliferation was assessed via a 5-ethynyl-2'-deoxyuridine (EdU)-Click 488 proliferation kit (Beyotime) according to the manufacturer's instructions. Next, 10 μM EdU was added to each well, and the mixture was incubated at 37°C in 5% CO_2 for 2 hours to label the proliferating cells. The nuclei were counterstained with 4',6-diamidino-2-phenylindole (DAPI). The cells were observed under a fluorescence microscope.

Cell Immunofluorescence (IF) Analysis

After the culture medium was removed, the fibroblasts were rinsed with PBS and fixed with 4% PFA for 20 minutes at room temperature. Then, the cells were permeabilized with 0.1% Triton X-100 for 15 minutes at room temperature, followed by blocking with 5% bovine serum albumin (BSA; Sigma–Aldrich, USA) for 1 h at room temperature. Next, the cells were incubated with a primary antibody against collagen I (1:2250; Abcam, ab138492) at 4°C overnight. The next day, the cells were incubated with a secondary antibody (Proteintech) and stained with DAPI. The cells were observed under a fluorescence microscope.

Collagen Gel Contraction Assay

The collagen gel contraction assay was conducted via a cell contraction assay kit (Cell Biolabs, USA, CBA-201). A 250 μL volume of the cell–collagen mixture was added to each well of a 24-well plate and incubated at 37°C for 1 hour to allow gel polymerization. After polymerization, 1 mL of culture medium was added on top of each collagen gel. After a two-day incubation period, the collagen gels were released from the bottom of the wells. The size of the collagen gels was measured on Day 3 and analyzed via ImageJ software.

Western Blot Analysis

Protein was extracted from fibroblasts, USCs and USC-sEVs via radioimmunoprecipitation assay lysis buffer supplemented with phenylmethylsulfonyl fluoride, proteinase and phosphatase inhibitors. The protein concentration was measured via a bicinchoninic acid (BCA) protein assay kit (Beyotime). The samples were mixed with 5× protein-loading buffer (Epizyme, China) and denatured at 95°C for 10 minutes. The proteins were separated via 10% or 12.5% sodium dodecyl sulfate–polyacrylamide gel electrophoresis (SDS–PAGE, Epizyme) and transferred onto 0.45 μm polyvinylidene fluoride membranes (PVDF, Millipore). The membranes were blocked with 5% nonfat milk for 1 hour and incubated with primary antibodies against CD63 (1:1000; Abcam, ab134045), TSG101 (1:1000; Abcam, ab125011), Hsp70 (1:1000; Abcam, ab181606), calnexin (1:1000; Abcam, ab133615), collagen I (1:1000; Abcam, ab138492), fibronectin (1:1000; Abcam, ab45688), GAPDH (1:1000; Abcam, ab181602), p38 MAPK (1:1000; CST, USA, 8690t), p-p38 MAPK (1:1000; CST, 4511t), Smad2/3 (1:1000; CST, 8685t), p-Smad2/3 (1:1000; Abcam, ab254407), decorin

(1:1000; Proteintech, 14667-1-ap) and DUSP3 (1:1000; Proteintech, 28284-1-ap) overnight at 4°C. The dilution ratio of the primary antibodies was 1:1000. The membranes were then incubated with horseradish peroxidase-conjugated secondary antibodies (Abcam) for 1 hour at room temperature. Finally, the proteins were visualized using enhanced chemiluminescence detection reagents (Beyotime) on an Amersham ImageQuant 800 imaging system (Cytiva, USA). Quantitative analysis of the immunoreactive bands was performed via ImageJ software.

Real-Time Quantitative Polymerase Chain Reaction (RT–qPCR) Analysis

Total RNA was extracted from cells and tissues via an RNAsimple Total RNA Kit (Tiangen, China, DP419) according to the manufacturer's instructions. Total RNA was reverse transcribed into cDNA via ABScript III Reverse Transcription Master Mix for qPCR (ABclonal, China, RK20428). RT–qPCR assays were performed via an Applied Biosystems Prism 7900HT (Thermo Scientific) with Universal SYBR Green Fast qPCR Mix (ABclonal, RK21203). Relative mRNA expression was normalized to that of GAPDH. The PCR primers used in this study are listed in Supplementary Table 1.

RNA Sequencing (RNA-Seq) Analysis

The RNA-seq analysis was conducted by OE Biotech Co., Ltd. (Shanghai, China). Total RNA was extracted via TRIzol reagent (Invitrogen, USA) according to the manufacturer's instructions. RNA purity and quantification were determined via a NanoDrop 2000 spectrophotometer (Thermo Scientific), and RNA integrity was assessed via an Agilent 2100 Bioanalyzer (Agilent Technologies, USA). The libraries were constructed via the VAHTS Universal V6 RNA-seq Library Prep Kit following the manufacturer's protocol. The libraries were sequenced on an Illumina NovaSeq 6000 platform.

Astral Data-Independent Acquisition (DIA) Proteomic Experiment

Proteomic analysis was performed by the Shanghai Bioprofile Technology Company (Shanghai, China).

Protein Preparation and Digestion

Proteins were extracted from USC-sEVs via SDT lysis buffer containing 4% sodium dodecyl sulfate, 100 mm dithiothreitol, 100 mm tris-hydrochloric acid at pH 8.0. The proteins were boiled for 3 minutes and then subjected to ultrasonication. After centrifugation at 16,000 × g for 15 minutes, the supernatant was collected and quantified via a BCA protein assay kit (Beyotime). An appropriate amount of protein from each sample was subjected to filter-aided sample preparation digestion. The steps were as follows: urea buffer containing detergent, dithiothreitol, and iodoacetamide was added to block reduced cysteine. The protein suspension was then digested with trypsin at a 50:1 ratio overnight at 37°C. The peptide mixtures were collected by centrifugation at 12,000 × g for 10 minutes and desalted via C18 StageTip for subsequent analysis.

Liquid Chromatography Coupled with Tandem Mass Spectrometry (LC–MS/MS) Analysis for DIA

For each sample, an appropriate amount of peptide was separated via a Vanquish Neo ultra high performance liquid chromatography system (Thermo Scientific). Buffer A consisted of 0.1% formic acid in water, and Buffer B consisted of 0.1% formic acid in 80% acetonitrile. The chromatographic column was equilibrated with 96% Buffer A. After sample injection into the trap column (PepMap Neo 5 μm C18 300 μm × 5 mm, Thermo Scientific), the peptides were separated via a μPAC Neo high-throughput column (Thermo Scientific). Peptides were then analyzed via an Orbitrap Astral mass spectrometer (Thermo Scientific) in DIA mode. The analysis duration was 24 minutes, with an electrospray voltage of 2.2 kV. The detection mode was positive ion mode, with a precursor ion scan range of 380–980 m/z. The primary mass spectrometry resolution was 240,000, with an automatic gain control target of 500% and a maximum injection time of 3 ms. The secondary mass spectrometry resolution was 80,000, with an AGC target of 500%, a maximum injection time of 3 ms, an RF lens of 40%, an MS2 activation type of higher-energy collisional dissociation, an isolation window of 2 Th, normalized collision energy of 25%, and a cycle time of 0.6 seconds.

Sequence Database Searching

The DIA mass spectrometry (MS) data were processed and analyzed via DIA-NN software for database searching and protein quantification. The key parameters and settings used for DIA mass spectrometric data analysis were as follows:

trypsin was utilized as the enzyme, with a maximum of one missed cleavage site allowed. Carbamidomethylation of cysteine was specified as a fixed modification, whereas oxidation of methionine and N-terminal acetylation were designated variable modifications. The database used was UniProtKB-*Homo sapiens* (Human) [9606]-204,141-20240326.fasta, following a target–reverse pattern. The database search results were filtered and exported with a <1% false discovery rate at both the peptide-spectrum-matched level and the protein level.

Bioinformatic Analysis

The proteins identified in USC-sEVs were compared with the published human proteins listed in the Vesiclepedia database. Venn diagram and Gene Ontology (GO) enrichment analyses were carried out via FunRich software (version 3.1.3). Canonical pathway analysis was performed with Ingenuity Pathway Analysis (IPA; Qiagen).

Statistical Analysis

Statistical analysis was performed via Student's *t*-test for single comparisons and analysis of variance (ANOVA) for multiple comparisons with GraphPad Prism 8 software. The results are expressed as the mean ± standard deviation. Differences with a P value < 0.05 were considered significant.

Results

Characterization of USCs and USC-sEVs

Approximately 7 days after initial seeding, the cell colonies were seen attaching to the bottom of the plates. Under a light microscope, USCs displayed a fibroblast-like or cobblestone morphology, which is typical of mesenchymal stem cells (MSCs) (Figure 1A). Flow cytometric analysis revealed that the USCs were positive for CD29, CD44, and CD73 and negative for CD45 and HLA-DR (Figure 1B). TEM analysis revealed that the USC-sEVs presented a characteristic cup-shaped morphology (Figure 1C). NTA further confirmed that the diameter of the USC-sEVs ranged from approximately 50 to 200 nm (Figure 1D). Western blot analysis revealed that the USC-sEVs were positive for CD63, TSG101 and Hsp70 but negative for calnexin, confirming that USC-sEVs were successfully isolated from the supernatant (Figure 1E).

Characterization and Biocompatibility of sEVs-Laden P-AM Scaffolds

For preparation of the sEVs-functionalized scaffold, a decellularized amniotic membrane (AM) was first produced via a unidirectional decellularization method. The resulting AM was smooth, milky white, and semitransparent (Figure 2B). PEI molecules were incorporated into the three-dimensional porous structure of the AM through multistep chemical processing, rendering the AM surface positively charged. The zeta potential of the vesicle surface was −16.85 mV (Figure S1). Owing to the negatively charged surface of the sEVs, USC-sEVs were electrostatically bound to the PEI-modified AM surface (Figure 2A).

The sEVs release experiment demonstrated that vesicles could be continuously released from the AM for up to one week, successfully creating an sEVs-functionalized scaffold capable of sustained USC-sEVs release (Figure 2C). To observe the duration of sEVs in vivo, sEVs were labeled with DiR and tracked for distribution in the rabbit vaginal wall using an in vivo fluorescence imaging system. On day 7, no fluorescent signal was detected in the sEVs group (Figure S2). However, fluorescent signals were still visible in the P-AM-sEVs group. These results suggested that P-AM-sEVs scaffold could provide sustained sEV delivery for over 7 days, potentially supporting wound healing over a longer period.

SEM revealed that the AM exhibited a three-dimensional porous structure with collagen fiber alignment, with pore diameters ranging from approximately 400 nm to 1 μm (Figure 2D). The three-dimensional porous structure of AM provides a conducive environment for cell attachment and proliferation, ensuring an adequate nutrient and oxygen supply. SEM images revealed that the fibroblasts adhered to the AM surface and exhibited a sheet-like morphology (Figure 2E). Live/dead cell assays demonstrated that after 36 hours of incubation with AMs, the majority of the fibroblasts remained viable, indicating that the AM material has good biocompatibility with the cells (Figure 2F).

Finally, considering that AMs, sEVs, and P-AM-sEVs scaffolds need to be in contact with the wound during in vivo use, their hemocompatibility was also evaluated. As shown in Figure S3, the hemolysis rates of AM extract, sEVs

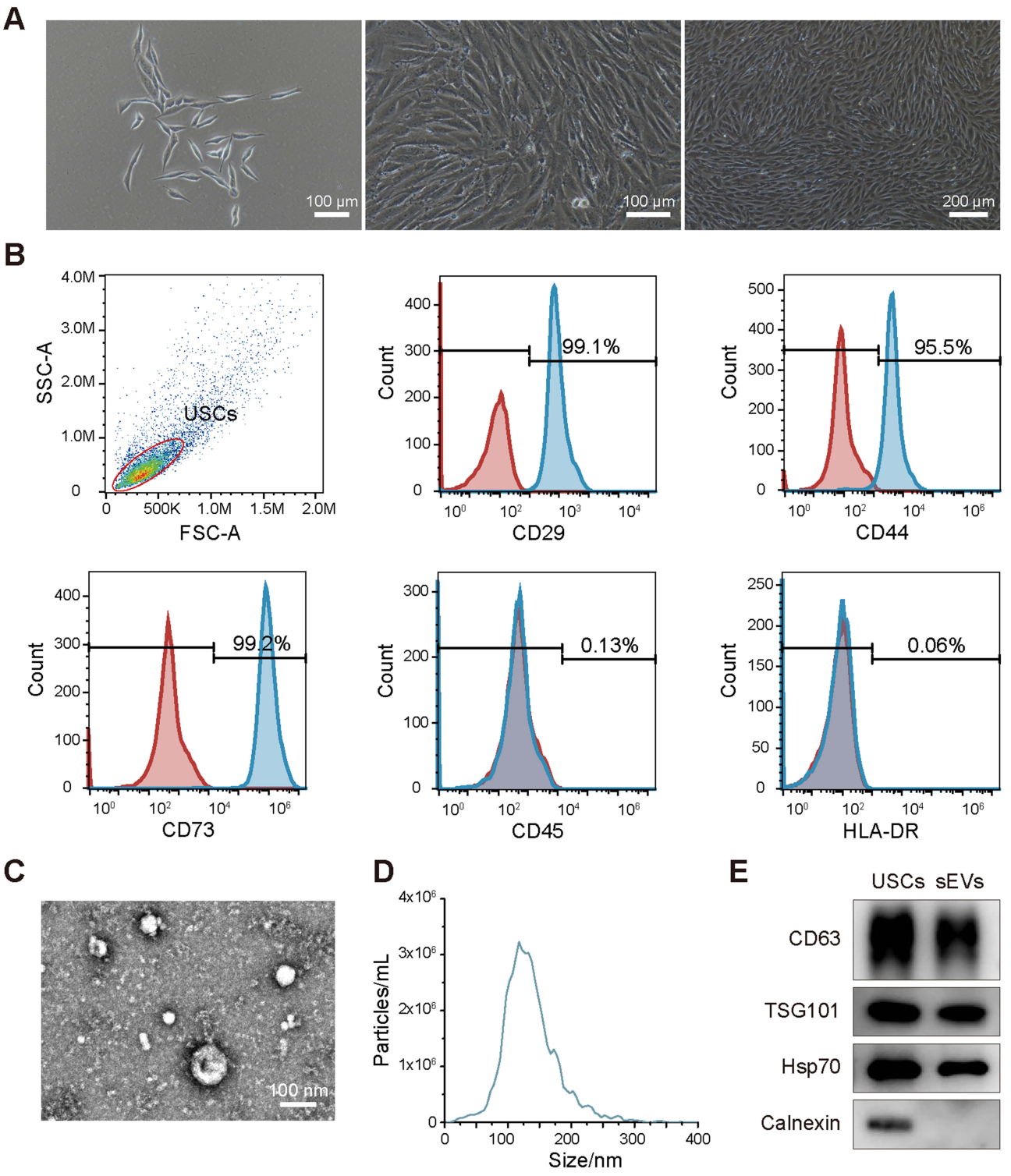

Figure 1 Characterization of USCs and USC-sEVs. (**A**) Morphological observation and growth of USCs. Scale bars: 100 μm (left and middle), 200 μm (right). (**B**) Flow cytometric analysis of CD29, CD44, CD45, CD73 and HLA-DR expression on USCs. (**C**) Morphology of USC-sEVs by TEM. Scale bar: 100 nm. (**D**) Particle size distribution of USC-sEVs by NTA. (**E**) Western blot analysis of the expression of CD63, TSG101, Hsp70 and calnexin.

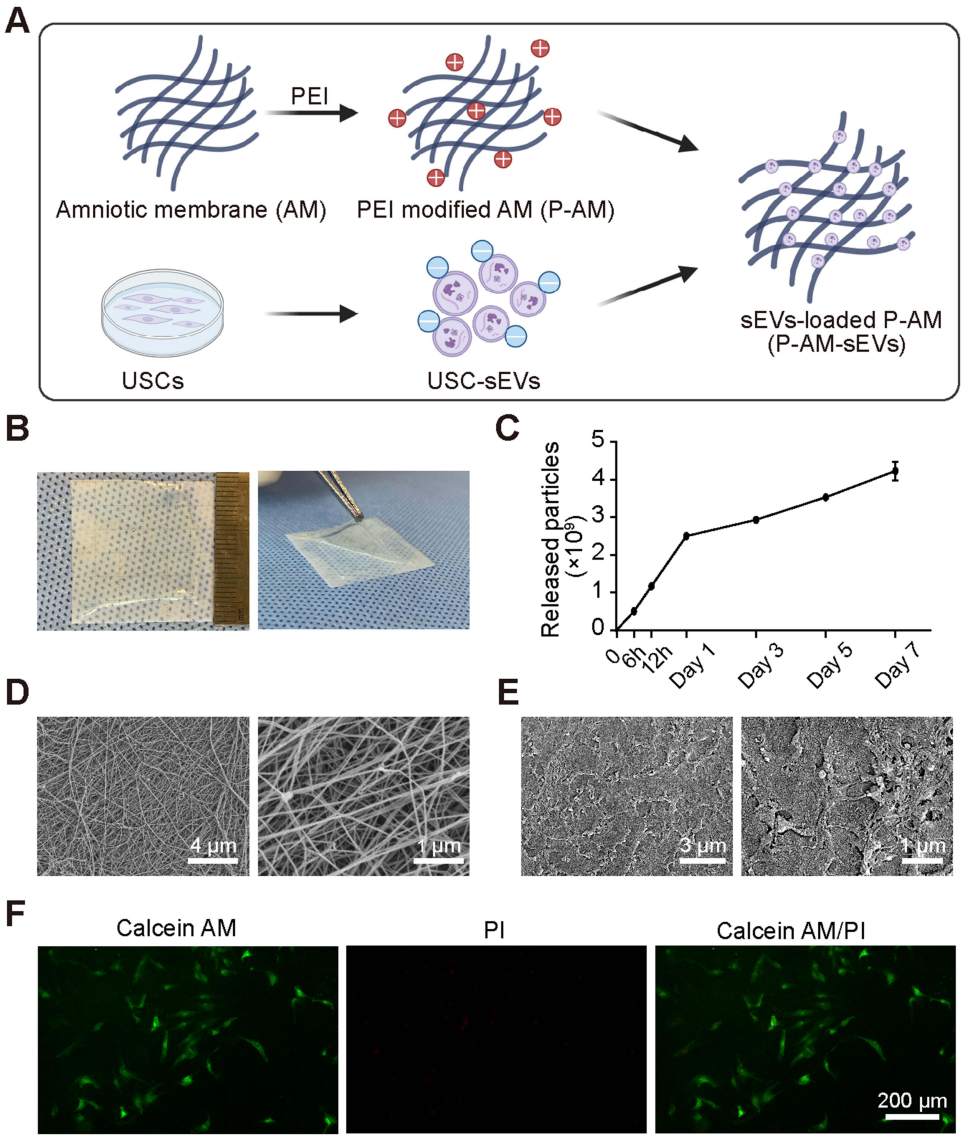

Figure 2 Characterization and biocompatibility of sEVs-laden P-AM scaffolds. (**A**) Schematic illustration of sEVs immobilization on AM scaffolds via electrostatic interactions. (**B**) Gross observation of the acellular amniotic membrane. (**C**) Curve of nanoparticles released from P-AM-sEVs over 7 days. (**D**) SEM images of AM fibers. Scale bars: 4 μm (left) and 1 μm (right). (**E**) SEM images of fibroblasts cultured on AM. Scale bars: 3 μm (left) and 1 μm (right). (**F**) Live/dead staining of fibroblasts cultured with AM. Scale bar: 200 μm.

dilution, and P-AM-sEVs extract were all below 5%, which met the international hemolysis assessment standards for medical materials/devices.

P-AM-sEVs Scaffolds Promoted Scarless Healing of Rabbit Vaginal Wounds by Promoting Epithelialization, Inhibiting Inflammation and Modulating Collagen Expression

To evaluate the therapeutic efficacy of the P-AM-sEVs scaffolds in promoting vaginal repair, we established a rabbit model of posterior vaginal wall defects, and the wound healing outcomes of each group were compared and analyzed (Figure 3A). During tissue retrieval, no notable implant reactions or signs of infection were observed, and the overall health of the rabbits was good. Macrophage infiltration is an important indicator of immune response and potential rejection following material implantation into a wound.[24] Compared to the PBS group, the P-AM-sEVs group showed

https://doi.org/10.2147/IJN.S499856

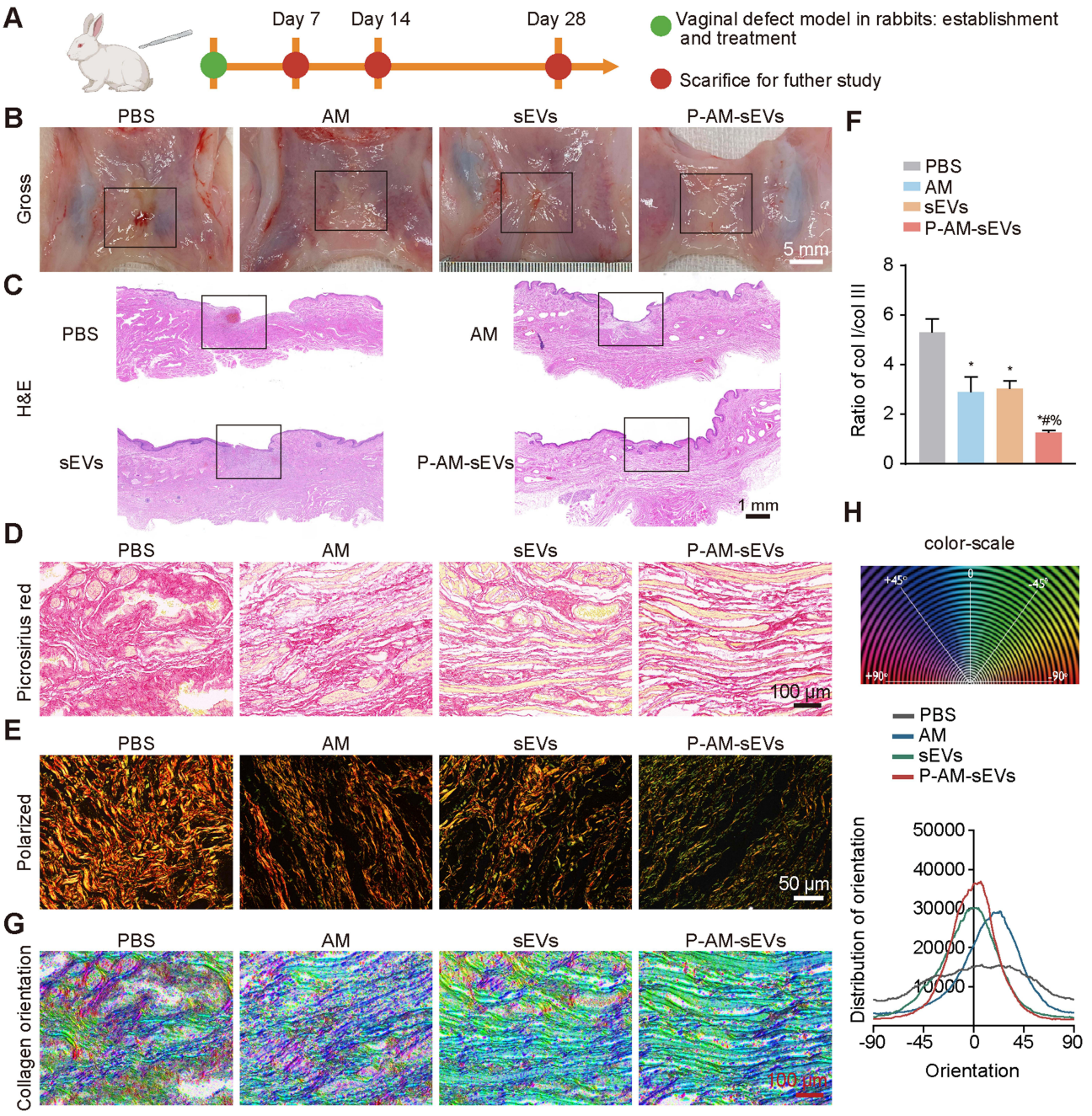

Figure 3 P-AM-sEVs scaffolds promoted scarless vaginal repair and regulated collagen deposition in rabbits on Day 14. (**A**) The scheme for the animal experiment. (**B**) Representative images of vaginal mucosa defects subjected to different treatments. Scale bar: 5 mm. (**C**) H&E staining of vaginal mucosa defects in each group. Scale bar: 1 mm. (**D**) Bright-field images of Picrosirius red-stained sections from the different groups. Scale bar: 100 μm. (**E** and **F**) Images of Picrosirius red-stained sections under polarized light and quantification of the collagen I/III ratio in each group. Scale bar: 50 μm. (**G** and **H**) The orientation of collagen fibers in Picrosirius red-stained sections was quantified via Orientation J software. The color representation reflects the various fiber orientations. Scale bar: 100 μm. *, $P < 0.05$, compared with the PBS group; #, $P < 0.05$, compared with the AM group; %, $P < 0.05$, compared with the sEVs group.

significantly fewer CD68-positive cells on Day 7, suggesting that P-AM-sEVs might effectively reduce macrophage infiltration and modulate local immune response (Figure S4).

Macroscopic observations after 14 days of different treatments revealed a major reduction in the wound area across all groups, with the P-AM-sEVs group showing the most rapid healing (Figure 3B). On Day 14 and Day 28, the surfaces of the wounds in the P-AM-sEVs group closely resembled those of normal vaginal mucosa, and were characterized by thin, soft, and smooth features (Figure S5). H&E staining was used to assess re-epithelialization and scar formation. On

Day 14, the PBS group presented a thin and discontinuous epithelium, pronounced inflammatory infiltration, and substantial scar formation, indicating poor wound healing (Figure 3C). In contrast, the other treatment groups exhibited strongly accelerated epithelialization and reduced scarring. Notably, the P-AM-sEVs group displayed a complete and well-organized epithelial structure with markedly reduced inflammation and scar formation, which was consistent with the macroscopic findings.

Collagen deposition and remodeling during vaginal wound healing were further investigated via Picrosirius red staining to assess the content and distribution of collagen I and collagen III. The results revealed a marked reduction in disorganized collagen fiber orientation in the treatment groups, suggesting a trend toward normal tissue remodeling (Figure 3D-H and Figure S6). Importantly, the ratio of collagen I to collagen III was significantly reduced in the sEVs and/or AM treatment groups, which might reduce scarring by modulating the ECM composition and ratio, a characteristic similar to fetal wound healing.

IHC analysis revealed a significant increase in collagen III expression in the treatment groups compared with the control group. The P-AM-sEVs group presented the highest level of collagen III expression, which was consistent with the Picrosirius red staining results (Figure 4A-B and Figure S7). Intervention with AMs and sEVs might increase wound healing by promoting collagen III deposition, increasing the stability and integrity of the tissue structure. IL-6 is a key regulator of the acute phase of inflammation. IHC staining revealed a significant reduction in the number and intensity of IL-6-positive cells in the treatment groups, suggesting that these treatments might promote wound healing by inhibiting the inflammatory response (Figure 4C-D).

RT–qPCR analysis revealed that, compared with those in the control group, the AM, sEVs, and combined treatment groups presented significantly lower expression of Col1A1, Col1A2 and TGF-β1, whereas the expression of Col3A1 and Smad7 was increased (Figure 4E). The expression of MMP2, MMP9, and IL-6 was also significantly reduced. These results suggested that AMs and sEVs, either alone or in combination, might promote scarless healing of vaginal wall wounds by modulating fibrosis-related genes and reducing the expression of inflammation-related genes and matrix remodeling-related enzymes.

USC-sEVs Inhibited TGF-β1-Induced Fibroblast Activation

The results of the EdU assay demonstrated that USC-sEVs treatment reduced the excessive proliferation of fibroblasts induced by TGF-β1 (Figure 5A-B). IF staining revealed that the expression of collagen I was increased in the TGF-β1-treated group, whereas treatment with USC-sEVs attenuated this increase (Figure 5C-D). Additionally, Western blot analysis confirmed that USC-sEVs treatment decreased the expression levels of collagen I and fibronectin induced by TGF-β1 (Figure 5E-F). The RT–qPCR results revealed a significant reduction in the expression of fibrosis-related genes, including Col1A1, MMP2, MMP14, ACTA2, and fibronectin, in the USC-sEVs-treated group (Figure 5G). Collagen gel contraction assays indicated that USC-sEVs treatment reduced the tension and contraction of the collagen matrix by inhibiting TGF-β1-induced fibroblast activation and contractile ability (Figure 5H-I). These findings support the antifibrotic effect of USC-sEVs.

USC-sEVs Modulated the Gene Expression Pattern in TGF-β1-Stimulated Fibroblasts

RNA-seq analysis was conducted to investigate the potential molecular mechanisms by which USC-sEVs regulate TGF-β1-induced fibroblast functions. Heatmaps and volcano plots revealed that USC-sEVs treatment significantly altered the differential gene expression profiles of TGF-β1-stimulated fibroblasts, with 196 upregulated genes (>2-fold, $p < 0.05$) and 323 downregulated genes (<0.5-fold, $p < 0.05$) (Figure 6A-B).

KEGG pathway analysis revealed that USC-sEVs treatment significantly inhibited fibrosis-related pathways, including the TGF-β signaling pathway, MAPK signaling pathway, ECM-receptor interaction, and cytokine–cytokine receptor interaction (Figure 6C and Figures S8 and S9). These pathways collectively contribute to tissue healing by regulating cell proliferation, migration, extracellular matrix remodeling, and inflammatory responses, which can influence scarless healing.[25–27] Gene set enrichment analysis (GSEA) indicated that the TGF-β and MAPK signaling pathways were significantly inhibited following USC-sEVs treatment, which was consistent with the KEGG analysis

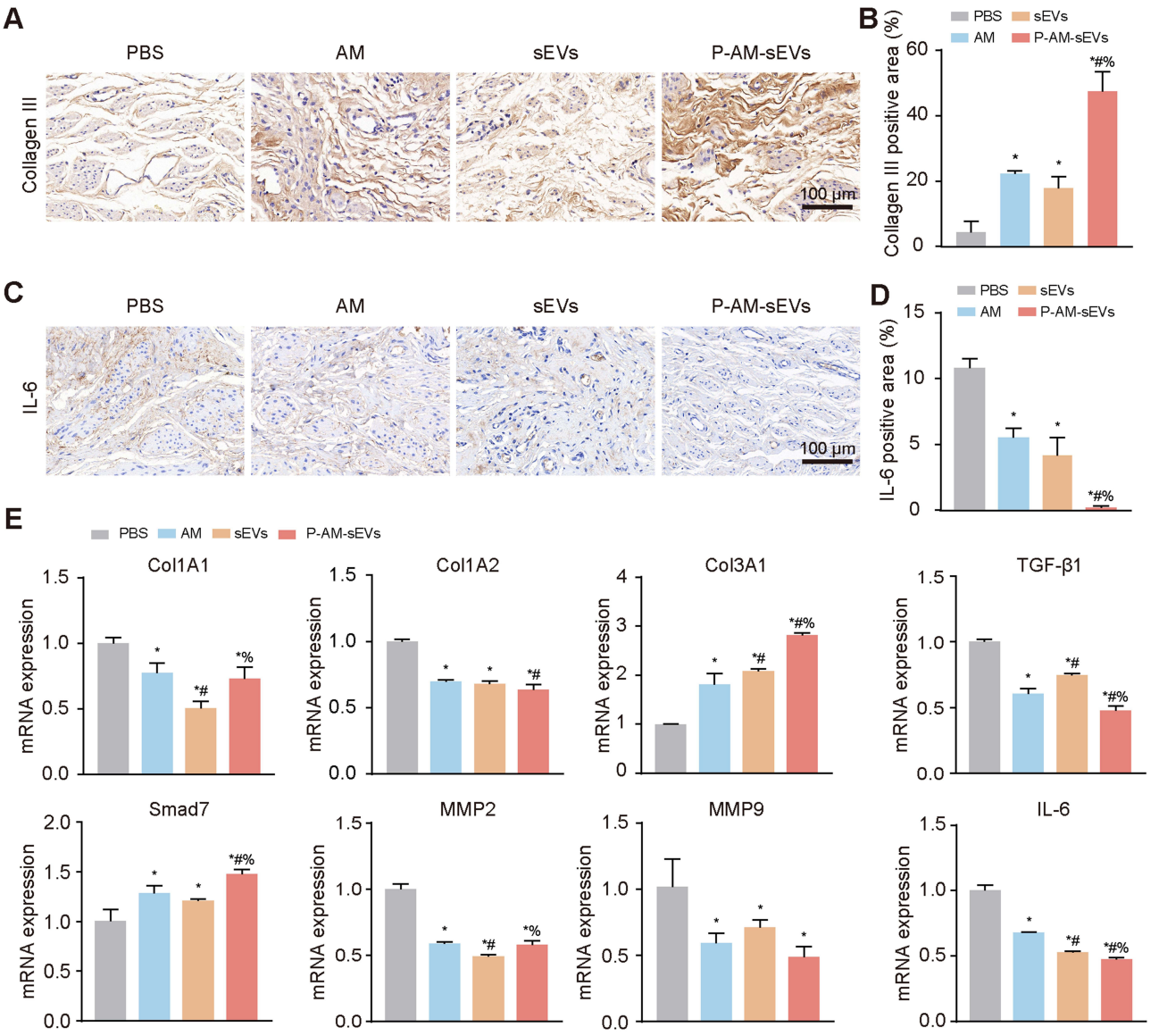

Figure 4 P-AM-sEVs scaffolds inhibited inflammation and reduced fibrosis in rabbits on Day 14. (**A** and **C**) IHC staining for collagen III and IL-6 after different treatments. Scale bar: 100 μm. (**B** and **D**) Quantification of IHC staining for collagen III and IL-6. n= 3 per group. (**E**) Quantification of the mRNA expression of fibrosis-related genes (Col1A1, Col1A2, Col3A1, TGF-β1, Smad7, MMP2, MMP9 and IL-6). n=3 per group. *, P < 0.05, compared with the PBS group; #, P < 0.05, compared with the AM group; %, P < 0.05, compared with the sEVs group.

results (Figure 6D-E). These findings suggest that USC-sEVs may inhibit fibroblast activation by modulating key fibrotic signaling pathways.

Previous studies have shown that the TGF-β and p38 MAPK signaling pathways are crucial in the development of fibrosis and scar formation.[28,29] Western blot analysis revealed that USC-sEVs treatment significantly reduced the phosphorylation levels of Smad2/3 and p38 MAPK in fibroblasts (Figure 6F-G). These data indicated that USC-sEVs might exert antifibrotic effects by inhibiting the TGF-β and p38 MAPK signaling pathways.

USC-sEVs Inhibited the TGF-β and p38 MAPK Signaling Pathways Through Delivery of Vesicle-Containing Decorin and DUSP3 Proteins to Fibroblasts

Extracellular vesicles can regulate biological processes in recipient cells by delivering encapsulated proteins.[30,31] DIA-based quantitative proteomic analysis revealed 2653 proteins in USC-sEVs, of which 2219 proteins were also found in the Vesiclepedia database, while 434 proteins were newly identified (Figure 7A).

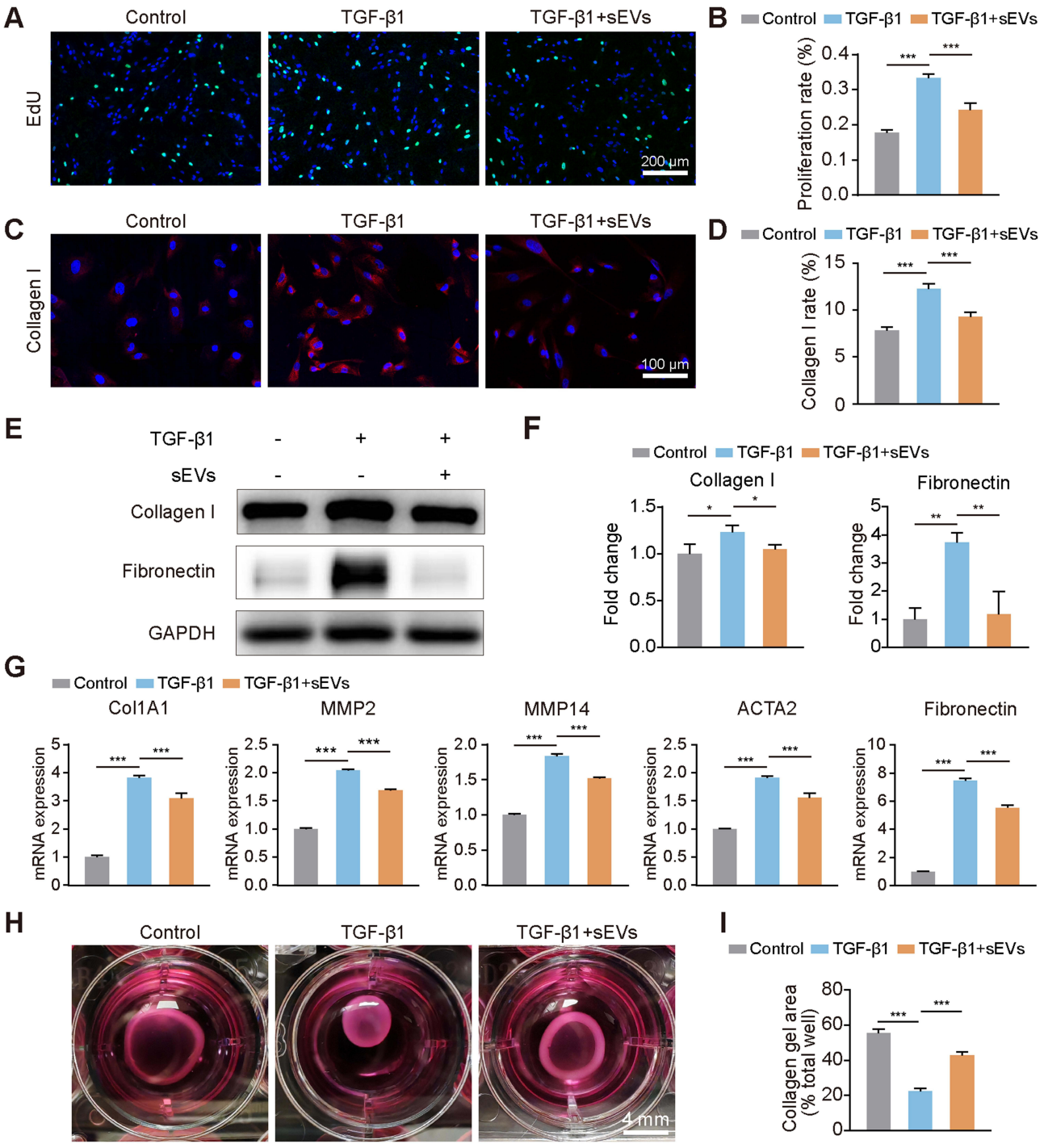

Figure 5 USC-sEVs attenuated the activation of TGF-β1-induced fibroblasts. (**A**) Representative images of EdU assays showing fibroblasts cocultured with TGF-β1 (10 ng/mL) and USC-sEVs (5×10^9 particles/mL). Scale bar: 200 μm. (**B**) Quantitative analysis of the proliferation rate of fibroblasts after different treatments. n=3 per group. (**C**) Representative images of IF staining of collagen I in fibroblasts at 48 h post-treatment. Scale bar: 100 μm. (**D**) Quantitative analysis of collagen I expression via IF staining. n=3 per group. (**E** and **F**) Western blot analysis of collagen I and fibronectin expression at 48 h post-treatment. n=3 per group. (**G**) Quantification of the mRNA expression of fibrosis-related genes (Col1A1, MMP2, MMP14, ACTA2 and fibronectin) after different treatments. n=3 per group. (**H** and **I**) Images and quantification of collagen gel contraction in different groups on Day 3. Scale bar: 4 mm. n=3 per group. *P < 0.05, **P < 0.01, ***P < 0.001.

IPA was used to identify the potential canonical signaling pathways associated with proteins found in USC-sEVs. These proteins are involved in various signaling pathways, including the Wnt/β-catenin, TGF-β, BMP, PI3K/ AKT, and ERK/MAPK pathways, all of which are closely linked to extracellular matrix organization and collagen degradation (Figure 7B).[32] GO analysis via FunRich software demonstrated that USC-sEV proteins play crucial roles in terms of

https://doi.org/10.2147/IJN.S499856

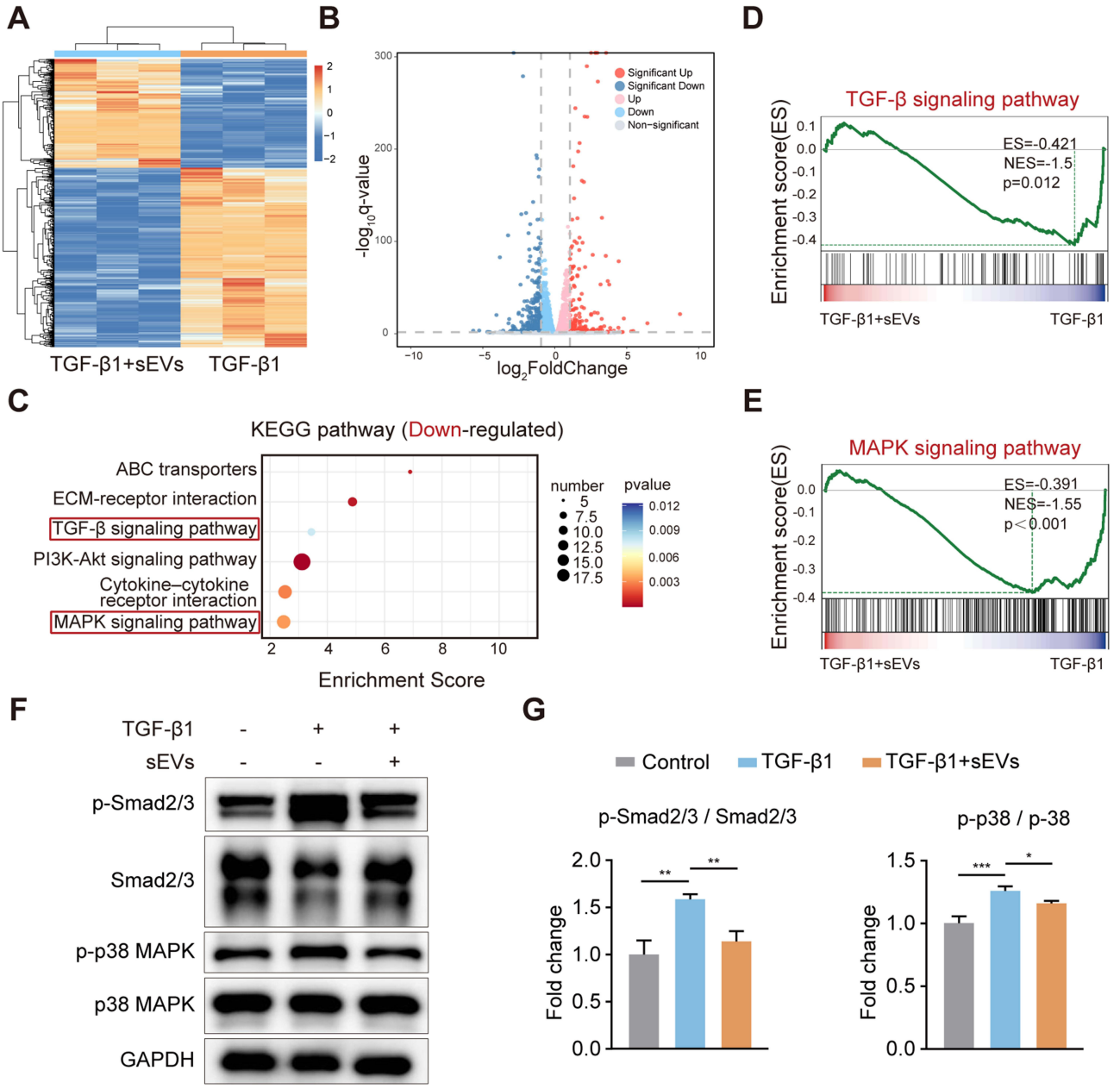

Figure 6 USC-sEVs modulated the gene expression pattern of fibroblasts under stimulation with TGF-β1. (**A** and **B**) Heatmap and volcano plot representing significantly differentially expressed genes in TGF-β1-induced fibroblasts treated with or without USC-sEVs. (**C**) KEGG analysis of pathways affected by USC-sEVs. (**D** and **E**) GSEA revealed enrichment scores for modules of the TGF-β signaling pathway and MAPK signaling pathway in fibroblasts following USC-sEVs treatment. (**F** and **G**) Western blot analysis of p-Smad2/3, Smad2/3, p-p38 MAPK and p38 MAPK expression in fibroblasts after USC-sEVs treatment. n=3 per group. *P < 0.05, **P < 0.01, ***P < 0.001.

cellular components, molecular functions, and biological processes (Figure 7C). Cellular component analysis indicated that the identified proteins predominantly originated from exosomes (45%). The identified proteins are involved in various molecular functions, including extracellular matrix structural constituent (3.5%), catalytic activity (5.8%), and structural constituent of cytoskeleton (2.2%) etc. Additionally, these proteins participate in biological processes such as protein metabolism (17%), metabolism (16.9%), and energy pathways (16.4%) etc.

Decorin is a known inhibitor of the TGF-β signaling pathway, whereas DUSP3 is responsible for dephosphorylating p38, thereby inhibiting the p38 MAPK signaling pathway.[33–36] Western blot analysis revealed that USC-sEVs were enriched with decorin and DUSP3 proteins (Figure 7D). Following USC-sEVs coincubation, the expression of decorin and DUSP3 in fibroblasts was significantly increased (Figure 7E). These results suggest that USC-sEVs can deliver

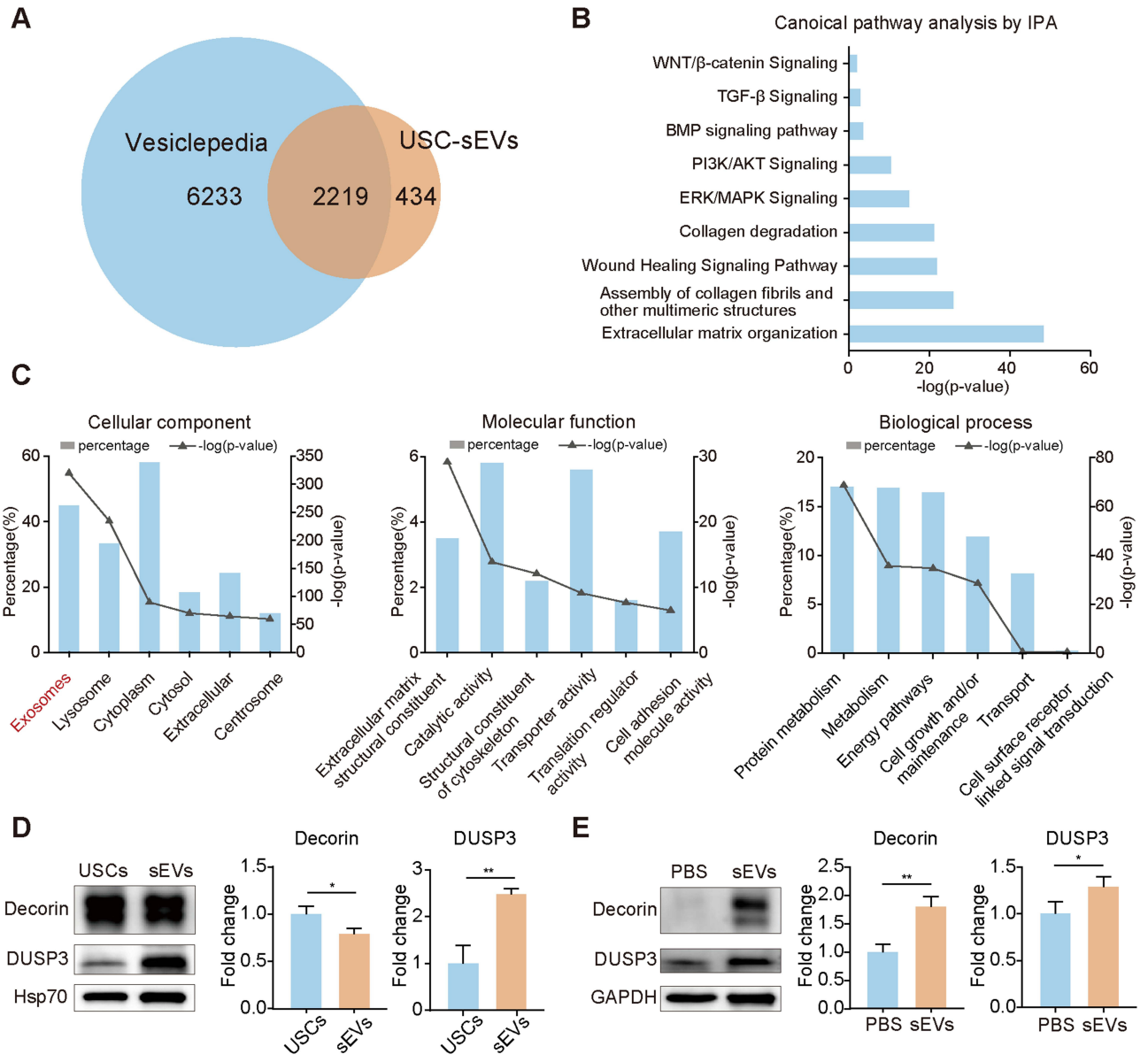

Figure 7 Proteomic analysis of USC-sEVs. (**A**) Venn diagram displaying the proportion of shared and unique proteins in USC-sEVs compared with those in the Vesiclepedia database. (**B**) IPA showing canonical pathway enrichment of proteins in USC-sEVs. (**C**) GO enrichment analyses of USC-sEVs proteins across the cellular component, molecular function, and biological process categories. (**D**) Western blot analysis of decorin and DUSP3 in USCs and USC-sEVs. n=3 per group. (**E**) Western blot analysis of decorin and DUSP3 in fibroblasts subjected to different treatments. n=3 per group. *P < 0.05, **P < 0.01.

decorin and DUSP3 to fibroblasts, thereby modulating the TGF-β and p38 MAPK signaling pathways, suggesting that USC-sEVs might be promising therapeutic reagents for inhibiting fibrosis and promoting scarless wound healing.

Discussion

Large-area vaginal defects following vaginoplasty are considered severe types of wound injury.[37] Although vaginal tissue has regenerative capabilities, restoring it to a normal state is often challenging. In this study, P-AM-sEVs, with their superior therapeutic effects and the advantages of autologous customization using USC-sEVs, might provide a novel treatment option for patients undergoing vaginal reconstructive surgery. Some studies have found that human umbilical MSCs (UC-MSCs) and bone marrow-derived MSCs could reconstruct damaged vaginal tissue in animal models.[38,39] However, the short retention time of directly transplanted stem cells at the site limited the duration of their therapeutic effects. The use of UC-MSCs alone in vaginal reconstruction in rats has been reported to provide better therapeutic

https://doi.org/10.2147/IJN.S499856

outcomes than SIS implantation alone or combined with UC-MSCs/SIS transplantation.[40] This might be related to chronic inflammation and collagen deposition caused by SIS implantation. Shi et al used 3D printing technology to construct a hydrogel scaffold containing decellularized ECM, gelatin methacrylate, and silk fibroin, which encapsulated UC-MSC-derived exosomes, to facilitate vaginal reconstruction in rats.[41] However, the varying degradation rates of the three components in the scaffold might result in instability during the repair process.

Scar formation is closely associated with the inflammatory environment, myofibroblast activity, and collagen deposition.[42] Studies have shown that collagen III-deficient mice exhibit increased levels of myofibroblast differentiation and scar formation, suggesting that collagen III plays a critical role in scar-free healing.[43] In our study, the combined application of AMs and sEVs increased the proportion of type III collagen and reduced the deposition of type I collagen, resembling the collagen remodeling pattern observed in fetal wound healing. Compared with adult wounds, fetal wound healing involves fewer inflammatory cells, which may lead to distinct profiles of cytokines and growth factors in the wound microenvironment.[44] Both in vivo and in vitro experiments indicated that the combination of sEVs and AMs significantly reduces inflammatory responses.

sEVs are known to encapsulate various bioactive components, including RNA, lipids, and proteins, from parent cells and mediate intercellular communication by transferring these active components.[45–47] Currently, there is relatively little research on the proteins enriched in USC-sEVs. In this study, we performed DIA proteomic analysis to explore the protein composition of USC-sEVs. We identified 2208 proteins, and GO analysis revealed that these vesicular proteins play critical roles in biological processes, including protein metabolism, energy pathways, cell growth, and signal transduction. Investigating these proteins and their mechanisms provides a foundation for developing therapeutic sEVs for scarless healing. Although our data suggest that the regulatory effects of USC-sEVs are mediated through the decorin and DUSP3 proteins, the potential involvement of other proteins cannot be excluded. For example, USC-sEVs contain matrix metalloproteinases (MMPs), including MMP1, MMP2, MMP7, MMP8, MMP9, MMP10, MMP14, and MMP15, which can directly participate in ECM degradation and remodeling.[48,49] Additionally, USC-sEVs are rich in members of the platelet-derived growth factor (PDGF) family, such as PDGFC and PDGFA, which play essential roles in wound healing and angiogenesis.[50–52] Notably, we also identified a novel set of 434 proteins not included in the current Vesiclepedia database.

The TGF-β signaling pathway has long been a focus of scar research.[53,54] Targeting TGF-β1 or its downstream signaling pathways (such as the Smad signaling pathway) may be an effective strategy to promote scarless healing.[29,55] However, owing to the complex regulatory mechanisms of TGF-β signaling in different types of cells, sustained or excessive inhibition could interfere with the normal wound healing process. The p38 MAPK signaling pathway plays a critical role in various diseases, including inflammatory diseases, cancer, cardiovascular diseases, nervous system diseases, and diabetes.[25,56–59] Targeted inhibition of the p38 MAPK signaling pathway, such as the use of the p38 MAPK inhibitor SB203580, has shown good potential in reducing the number of hypertrophic scars in the skin.[60] There is also substantial crosstalk between the TGF-β and p38 MAPK signaling pathways.[61–63] Further study of the interactions among target points and their related regulatory processes can provide new research avenues for the treatment of wound healing. Although our data indicated that the regulatory effects of USC-sEVs were partly achieved through the TGF-β and p38 MAPK signaling pathways, the achievement of scarless healing actually involves the complex regulation of multiple signaling pathways. IPA suggested that various proteins identified in USC-sEVs are involved in multiple canonical signaling pathways, which act synergistically. Therefore, the potential mechanisms by which USC-sEVs promote scarless healing require further investigation.

In conclusion, the effectiveness of P-AM-sEVs biological scaffolds in promoting scarless healing suggests potential directions for future scaffold design: optimizing scaffold functionality by integrating elements that regulate collagen dynamics, inhibiting key fibrotic pathways, and promoting favorable immune responses. These strategies could involve the use of different biomaterials, growth factors, or sEVs derived from other cell types, each tailored to meet the specific repair needs of the target tissue. These improvements will lead to new prospects for the clinical application of scarless tissue repair.

Conclusion

In this study, we developed a novel acellular tissue-engineered approach for vaginal reconstruction. The AM scaffold loaded with USC-sEVs promoted scar-free healing of the vaginal wall in rabbits by accelerating epithelialization, suppressing immune responses, and modulating collagen deposition. These findings not only provide a new therapeutic strategy for vaginal scar-free healing but also offer novel insights for tissue-engineering repair of other organs, such as the urethra, bladder, and skin. Further investigation revealed that the decorin/TGF-β and DUSP3/p38 MAPK signaling pathways were potential molecular mechanisms through which USC-sEVs inhibited fibrosis. The in vitro mechanistic exploration not only provides a theoretical basis for the clinical translation of this treatment but also offers important experimental evidence for future optimization of therapeutic strategies.

Abbreviations

SIS, small intestinal submucosa; sEVs, small extracellular vesicles; USCs, urine-derived stem cells; USC-sEVs, USC-derived sEVs; AM, amniotic membrane; ECM, extracellular matrix; PBS, phosphate-buffered saline; FBS, fetal bovine serum; BSA, bovine serum albumin; TEM, transmission electron microscopy; NTA, nanoparticle tracking analysis; PEI, polyethyleneimine; EDC, 1-ethyl-3-(3-dimethylaminopropyl) carbodiimide; NHS, N-hydroxysuccinimide; SEM, scanning electron microscopy; calcein AM, calcein acetoxymethyl ester; PI, propidium iodide; PFA, paraformaldehyde; H&E, hematoxylin and eosin; IHC, immunohistochemistry; IL-6, Interleukin-6; IF, immunofluorescence; TGF-β1, transforming growth factor beta 1; EdU, 5-ethynyl-2'-deoxyuridine; DAPI, 4', 6-diamidino-2-phenylindole; BCA, bicinchoninic acid; SDS–PAGE, sodium dodecyl sulfate–polyacrylamide gel electrophoresis; PVDF, polyvinylidene fluoride membranes; RT–qPCR, real-time quantitative polymerase chain reaction; RNA-Seq, RNA sequencing; DIA, data-independent acquisition; LC–MS/MS, liquid chromatography coupled with tandem mass spectrometry; MS, mass spectrometry; GO, Gene Ontology; IPA, Ingenuity Pathway Analysis; ANOVA, analysis of variance; MSCs, mesenchymal stem cells; UC-MSCs, human umbilical mesenchymal stem cells; MMPs, matrix metalloproteinases; PDGF, platelet-derived growth factor.

Data Sharing Statement

The datasets used and/or analyzed during the current study are available from the corresponding author upon reasonable request.

Ethics Approval

The animal experiments in this study were approved by the Animal Care and Use Committee of Shanghai Sixth People's Hospital (No. 2023-0517). All animal experiments were conducted in accordance with the ethical review of animal welfare for laboratory animals (GB/T 35892–2018). The Ethics approval for the acquisition of human urine and amniotic membrane was obtained from by the Independent Ethics Committee of Shanghai Sixth People's Hospital (Approval code: 2018-KY-035(K)). All procedures were conducted in accordance with the Declaration of Helsinki.

Author Contributions

All authors made a significant contribution to the work reported, whether that is in the conception, study design, execution, acquisition of data, analysis and interpretation, or in all these areas; took part in drafting, revising or critically reviewing the article; gave final approval of the version to be published; have agreed on the journal to which the article has been submitted; and agree to be accountable for all aspects of the work.

Funding

This work was supported by the National Natural Science Foundation of China (Grant NO. 81771523, 82071631).

Disclosure

The authors report no conflicts of interest in this work.

References

1. Fedele F, Bulfoni A, Parazzini F, et al. Neovagina creation methods in Müllerian anomalies and risk of malignancy: insights from a systematic review. *Arch Gynecol Obstet*. 2024;309(3):801–812. doi:10.1007/s00404-023-07086-6
2. Kölle A, Taran FA, Rall K, et al. Neovagina creation methods and their potential impact on subsequent uterus transplantation: a review. *BJOG*. 2019;126(11):1328–1335. doi:10.1111/1471-0528.15888
3. Kisu I, Iida M, Shiraishi T, et al. Novel vaginoplasty technique involving the use of peritoneal flaps during laparoscopic radical hysterectomy for early-stage cervical cancer. *J Gynecol Oncol*. 2022;33(2):e19. doi:10.3802/jgo.2022.33.e19
4. Bene NC, Ferrin PC, Xu J, et al. Tissue options for construction of the neovaginal canal in gender-affirming vaginoplasty. *J Clin Med Res*. 2024;13(10):2760. doi:10.3390/jcm13102760
5. Ferrando CA. Updates on feminizing genital affirmation surgery (vaginoplasty) techniques. *Neurourol Urodyn*. 2023;42(5):931–938. doi:10.1002/nau.25088
6. Zhu L, Zhou H, Sun Z, et al. Anatomic and sexual outcomes after vaginoplasty using tissue-engineered biomaterial graft in patients with Mayer-Rokitansky-Küster-Hauser syndrome: a new minimally invasive and effective surgery. *J Sex Med*. 2013;10(6):1652–1658. doi:10.1111/jsm.12143
7. Xu H, Hou S, Ruan Z, et al. Comparing anatomical and functional outcomes of two neovaginoplasty techniques for Mayer-Rokitansky-Küster-Hauser syndrome: a ten-year retrospective study with swine small intestinal submucosa and homologous skin grafts. *Ther Clin Risk Manag*. 2023;19:557–565. doi:10.2147/tcrm.S415672
8. Nguyen T, Gundogdu G, Bottini C, et al. Evaluation of bi-layer silk fibroin grafts for inlay vaginoplasty in a rat model. *Tissue Eng Regen Med*. 2024;21(7):985–994. doi:10.1007/s13770-024-00653-1
9. Ho MH, Heydarkhan S, Vernet D, et al. Stimulating vaginal repair in rats through skeletal muscle-derived stem cells seeded on small intestinal submucosal scaffolds. *Obstet Gynecol*. 2009;114(2 Pt 1):300–309. doi:10.1097/AOG.0b013e3181af6abd
10. Stojanovic B, Horwood G, Joksic I, et al. Management of vaginoplasty canal complications. *Curr Opin Urol*. 2024;34(5):336–343. doi:10.1097/mou.0000000000001204
11. Li JS, Crane CN, Santucci RA. Vaginoplasty tips and tricks. *Int Braz J Urol*. 2021;47(2):263–273. doi:10.1590/s1677-5538.Ibju.2020.0338
12. Shao S, Wang X, Lei X, et al. Psychological intervention in women with Mayer-Rokitansky-Küster-Hauser syndrome after artificial vaginoplasty: a prospective study. *Int Urogynecol J*. 2022;33(3):723–729. doi:10.1007/s00192-022-05075-y
13. Liao Z, Tong B, Zhang X, et al. Selective cargo sorting in stem cell-derived small extracellular vesicles: impact on therapeutic efficacy for intervertebral disc degeneration. *Clin Transl Med*. 2023;13(12):e1494. doi:10.1002/ctm2.1494
14. Lee CS, Lee M, Na K, et al. Stem cell-derived extracellular vesicles for cancer therapy and tissue engineering applications. *Mol Pharm*. 2023;20(11):5278–5311. doi:10.1021/acs.molpharmaceut.3c00376
15. Sun Y, Zhao H, Yang S, et al. Urine-derived stem cells: promising advancements and applications in regenerative medicine and beyond. *Heliyon*. 2024;10(6):e27306. doi:10.1016/j.heliyon.2024.e27306
16. Zhang W, Hu J, Huang Y, et al. Urine-derived stem cells: applications in skin, bone and articular cartilage repair. *Burns Trauma*. 2021;9:tkab039. doi:10.1093/burnst/tkab039.
17. Moore AL, Marshall CD, Barnes LA, et al. Scarless wound healing: transitioning from fetal research to regenerative healing. *Wiley Interdiscip Rev-Dev Biol*. 2018;7(2):e309. doi:10.1002/wdev.309
18. Zhou H, Wang L, Zhang C, et al. Feasibility of repairing full-thickness skin defects by iPSC-derived epithelial stem cells seeded on a human acellular amniotic membrane. *Stem Cell Res Ther*. 2019;10(1):155. doi:10.1186/s13287-019-1234-9
19. Han Y, Ren QL. Does probiotics work for bacterial vaginosis and vulvovaginal candidiasis. *Curr Opin Pharmacol*. 2021;61:83–90. doi:10.1016/j.coph.2021.09.004
20. Fénelon M, Catros S, Meyer C, et al. Applications of human amniotic membrane for tissue engineering. *Membranes*. 2021;11(6):387. doi:10.3390/membranes11060387
21. Li X, Liao J, Su X, et al. Human urine-derived stem cells protect against renal ischemia/reperfusion injury in a rat model via exosomal miR-146a-5p which targets IRAK1. *Theranostics*. 2020;10(21):9561–9578. doi:10.7150/thno.42153
22. Cao YM, Liu MY, Xue ZW, et al. Surface-structured bacterial cellulose loaded with hUSCs accelerate skin wound healing by promoting angiogenesis in rats. *Biochem Biophys Res Commun*. 2019;516(4):1167–1174. doi:10.1016/j.bbrc.2019.06.161
23. Wu RY, Huang CS, Wu QK, et al. Exosomes secreted by urine-derived stem cells improve stress urinary incontinence by promoting repair of pubococcygeus muscle injury in rats. *Stem Cell Res Ther*. 2019;10(1):80. doi:10.1186/s13287-019-1182-4
24. Wang W, Liu Z, Zhu J, et al. Macrophage tracking with USPIO imaging and T2 mapping predicts immune rejection of transplanted stem cells. *Sci Rep*. 2024;14(1):29162. doi:10.1038/s41598-024-80750-2
25. Bengal E, Aviram S, Hayek T. p38 MAPK in glucose metabolism of skeletal muscle: beneficial or harmful? *Int J Mol Sci*. 2020;21(18):6480. doi:10.3390/ijms21186480
26. Bhattacharya D, Tiwari R, Bhatia T, et al. Accelerated and scarless wound repair by a multicomponent hydrogel through simultaneous activation of multiple pathways. *Drug Deliv Transl Res*. 2019;9(6):1143–1158. doi:10.1007/s13346-019-00660-z
27. Kong X, Jiang S, He Q, et al. TLR8 aggravates skin inflammation and fibrosis by activating skin fibroblasts in systemic sclerosis. *Rheumatology*. 2024;63(6):1710–1719. doi:10.1093/rheumatology/kead456
28. Li Y, Zhang W, Gao J, et al. Adipose tissue-derived stem cells suppress hypertrophic scar fibrosis via the p38/MAPK signaling pathway. *Stem Cell Res Ther*. 2016;7(1):102. doi:10.1186/s13287-016-0356-6
29. Zhang T, Wang XF, Wang ZC, et al. Current potential therapeutic strategies targeting the TGF-β/Smad signaling pathway to attenuate keloid and hypertrophic scar formation. *Biomed Pharmacother*. 2020;129:110287. doi:10.1016/j.biopha.2020.110287
30. Choi JS, Cho WL, Choi YJ, et al. Functional recovery in photo-damaged human dermal fibroblasts by human adipose-derived stem cell extracellular vesicles. *J Extracell Vesicles*. 2019;8(1):1565885. doi:10.1080/20013078.2019.1565885
31. Upadhya R, Madhu LN, Attaluri S, et al. Extracellular vesicles from human iPSC-derived neural stem cells: miRNA and protein signatures, and anti-inflammatory and neurogenic properties. *J Extracell Vesicles*. 2020;9(1):1809064. doi:10.1080/20013078.2020.1809064
32. Moretti L, Stalfort J, Barker TH, et al. The interplay of fibroblasts, the extracellular matrix, and inflammation in scar formation. *J Biol Chem*. 2022;298(2):101530. doi:10.1016/j.jbc.2021.101530

33. Wang S, Qu Y, Fang X, et al. Decorin: a potential therapeutic candidate for ligamentum flavum hypertrophy by antagonizing TGF-β1. *Exp Mol Med*. 2023;55(7):1413–1423. doi:10.1038/s12276-023-01023-y
34. Eremenko EE, Kwan PO, Ding J, et al. The effects of TGF-β1 and IFN-α2b on decorin, decorin isoforms and type I collagen in hypertrophic scar dermal fibroblasts. *Wound Repair Regen*. 2024;32(2):135–145. doi:10.1111/wrr.13155
35. Monteiro LF, Ferruzo PYM, Russo LC, et al. DUSP3/VHR: a druggable dual phosphatase for human diseases. *Rev Physiol Biochem Pharmacol*. 2019;176:1–35. doi:10.1007/112_2018_12
36. Burton JC, Antoniades W, Okalova J, et al. Atypical p38 signaling, activation, and implications for disease. *Int J Mol Sci*. 2021;22(8):4183. doi:10.3390/ijms22084183
37. Schardein JN, Zhao LC, Nikolavsky D. Management of vaginoplasty and phalloplasty complications. *Urol Clin North Am*. 2019;46(4):605–618. doi:10.1016/j.ucl.2019.07.012
38. Menachem-Zidon OB, Gropp M, Reubinoff B, et al. Mesenchymal stem cell transplantation improves biomechanical properties of vaginal tissue following full-thickness incision in aged rats. *Stem Cell Rep*. 2022;17(11):2565–2578. doi:10.1016/j.stemcr.2022.09.005
39. Ma Y, Zhang Y, Chen J, et al. Mesenchymal stem cell-based bioengineered constructs enhance vaginal repair in ovariectomized rhesus monkeys. *Biomaterials*. 2021;275:120863. doi:10.1016/j.biomaterials.2021.120863
40. Zhang Y, Zhu Z, Hua K, et al. Umbilical cord-derived mesenchymal stem cell transplantation in vaginal replacement in vitro and in a rat model. *Am J Transl Res*. 2018;10(11):3762–3772.
41. Shi W, Zheng J, Zhang J, et al. Desktop-stereolithography 3D printing of a decellularized extracellular matrix/mesenchymal stem cell exosome bioink for vaginal reconstruction. *Tissue Eng Regen Med*. 2024;21(6):943–957. doi:10.1007/s13770-024-00649-x
42. Lee SH, An S, Ryu YC, et al. Adhesive hydrogel patch-mediated combination drug therapy induces regenerative wound healing through reconstruction of regenerative microenvironment. *Adv Healthc Mater*. 2023;12(18):e2203094. doi:10.1002/adhm.202203094
43. Volk SW, Wang Y, Mauldin EA, et al. Diminished type III collagen promotes myofibroblast differentiation and increases scar deposition in cutaneous wound healing. *Cells Tissues Organs*. 2011;194(1):25–37. doi:10.1159/000322399
44. Walraven M, Gouverneur M, Middelkoop E, et al. Altered TGF -β signaling in fetal fibroblasts: what is known about the underlying mechanisms? *Wound Repair Regen*. 2014;22(1):3–13. doi:10.1111/wrr.12098
45. Kalluri R, LeBleu VS. The biology, function, and biomedical applications of exosomes. *Science*. 2020;367(6478):eaau6977. doi:10.1126/science.aau6977
46. Gurunathan S, Kang MH, Kim JH. A comprehensive review on factors influences biogenesis, functions, therapeutic and clinical implications of exosomes. *Int J Nanomed*. 2021;16:1281–1312. doi:10.2147/ijn.S291956
47. Isaac R, Reis FCG, Ying W, et al. Exosomes as mediators of intercellular crosstalk in metabolism. *Cell Metab*. 2021;33(9):1744–1762. doi:10.1016/j.cmet.2021.08.006
48. Cabral-Pacheco GA, Garza-Veloz I, Castruita-De la Rosa C, et al. The roles of matrix metalloproteinases and their inhibitors in human diseases. *Int J Mol Sci*. 2020;21(24):9739. doi:10.3390/ijms21249739
49. Wang X, Khalil RA. Matrix metalloproteinases, vascular remodeling, and vascular disease. *Adv Pharmacol*. 2018;81:241–330. doi:10.1016/bs.apha.2017.08.002
50. Jian K, Yang C, Li T, et al. PDGF-BB-derived supramolecular hydrogel for promoting skin wound healing. *J Nanobiotechnol*. 2022;20(1):201. doi:10.1186/s12951-022-01390-0
51. Lee C, Li X. Platelet-derived growth factor-C and -D in the cardiovascular system and diseases. *Mol Asp Med*. 2018;62:12–21. doi:10.1016/j.mam.2017.09.005
52. Wang Y, Ding C, Zhao Y, et al. Sodium alginate/poly (vinyl alcohol)/taxifolin nanofiber mat promoting diabetic wound healing by modulating the inflammatory response, angiogenesis, and skin flora. *Int J Biol Macromol*. 2023;252:126530. doi:10.1016/j.ijbiomac.2023.126530
53. Yang M, Zhang Y, Fang C, et al. Urine-microenvironment-initiated composite hydrogel patch reconfiguration propels scarless memory repair and reinvigoration of the urethra. *Adv Mater*. 2022;34(14):e2109522. doi:10.1002/adma.202109522
54. Lee JH, Massagué J. TGF-β in developmental and fibrogenic EMTs. *Semin Cancer Biol*. 2022;86(Pt 2):136–145. doi:10.1016/j.semcancer.2022.09.004
55. Ren LL, Li XJ, Duan TT, et al. Transforming growth factor-β signaling: from tissue fibrosis to therapeutic opportunities. *Chem Biol Interact*. 2023;369:110289. doi:10.1016/j.cbi.2022.110289
56. Yong HY, Koh MS, Moon A. The p38 MAPK inhibitors for the treatment of inflammatory diseases and cancer. *Expert Opin Investig Drugs*. 2009;18(12):1893–1905. doi:10.1517/13543780903321490
57. Martínez-Limón A, Joaquin M, Caballero M, et al. The p38 pathway: from biology to cancer therapy. *Int J Mol Sci*. 2020;21(6):1913. doi:10.3390/ijms21061913
58. Reustle A, Torzewski M. Role of p38 MAPK in atherosclerosis and aortic valve sclerosis. *Int J Mol Sci*. 2018;19(12):3761. doi:10.3390/ijms19123761
59. Wei TH, Hsieh CL. Effect of acupuncture on the p38 signaling pathway in several nervous system diseases: a systematic review. *Int J Mol Sci*. 2020;21(13):4693. doi:10.3390/ijms21134693
60. Li Q, Chen H, Liu Y, et al. Osteomodulin contributes to keloid development by regulating p38 MAPK signaling. *J Dermatol*. 2023;50(7):895–905. doi:10.1111/1346-8138.16777
61. Zhou X, Guo Y, Yang K, et al. The signaling pathways of traditional Chinese medicine in promoting diabetic wound healing. *J Ethnopharmacol*. 2022;282:114662. doi:10.1016/j.jep.2021.114662
62. Boye A, Kan H, Wu C, et al. MAPK inhibitors differently modulate TGF-β/Smad signaling in HepG2 cells. *Tumor Biol*. 2015;36(5):3643–3651. doi:10.1007/s13277-014-3002-x
63. Terai K, Call MK, Liu H, et al. Crosstalk between TGF-beta and MAPK signaling during corneal wound healing. *Invest Ophthalmol Vis Sci*. 2011;52(11):8208–8215. doi:10.1167/iovs.11-8017